Hindawi
Geofluids
Volume 2019, Article ID 7639159, 11 pages
https://doi.org/10.1155/2019/7639159

Research Article

Force-Fracture Characteristics of the Roof above Goaf in a Steep Coal Seam: A Case Study of Xintie Coal Mine

Hong-sheng Tu,[1,2,3] **Shi-hao Tu**,[1,2] **De-fu Zhu**,[1,2] **Ding-yi Hao**,[1,2] **and Kai-jun Miao**[1,2]

[1]*State Key Laboratory of Coal Resources and Safe Mining, China University of Mining and Technology, Xuzhou, Jiangsu 221116, China*
[2]*Key Laboratory of Deep Coal Resource Mining, Ministry of Education, China University of Mining and Technology, Xuzhou, Jiangsu 221116, China*
[3]*Chongqing Energy Investment Group Science and Technology Co. Ltd, Chongqing Energy, Chongqing 401121, China*

Correspondence should be addressed to Shi-hao Tu; tsh@cumt.edu.cn

Received 22 June 2018; Revised 4 January 2019; Accepted 10 January 2019; Published 7 March 2019

Guest Editor: Wen Wang

After coal is extracted from a working face in a steep coal seam (SCS), the immediate roof tends to cave in and refill the lower part of the goaf. Based on the geological conditions of a work area in a SCS and the characteristics of roof caving, this study proposed a formula for the width of the backfill in the goaf and analyzed the main factors influencing it. Based on the small-deflection theory for elastic thin plates, a working face model was created for the mechanical analysis of the main roof above a SCS before the roof fractures for the first time. Then, a roof deflection equation was derived for the estimation roof deformation under the action of both the load from overlying strata and the support provided by the backfill in the goaf. The theoretical analysis combined with the actual operational parameters at the Zuoqipian working face in #49 seam of Xintie Coal Mine shows that the maximum roof deflection is around 0.8 m and occurs at a location 39 m from the upper end of the working face. Fractures will first develop in the upper sections of the frontal and rear walls of the face and the middle of the upper suspended roof due to tension or shearing and ultimately form an *E*-shaped pattern. The measured support pressure and the roof deformation obtained by theoretical analysis show a similar distribution pattern, indirectly confirming the accuracy of the theoretical results.

1. Introduction

The roof of a working face consists of the immediate roof and the main roof. The immediate roof is normally composed of thin and soft rock strata. It is thus able to fall easily as mining progresses and thus has little influence on the mining operation. The main roof is usually made up of thick and hard rock strata. As the main roof has a long suspended section behind the face, its fracture has a great influence on the mining operation and is often accompanied by strong strata behavior, making it difficult to control the surrounding rock. Therefore, there is an emphasis on controlling the fall of the main roof during mining. To study strata behavior at a working face and develop roof control measures, it is necessary first to understand the stress-deformation-fracture characteristics of the main roof [1]. A lot of research has looked at the stress-deformation-fracture characteristics of the main roof above flat or gently dipping coal seams and reached many useful conclusions. For a steep coal seam (typically defined as a seam dipping at an angle larger than 45° [2]), the in situ stress in the main roof can be divided into two components: a shear component, which is parallel to the dip direction, and a normal component, which is perpendicular to the seam. The shear component is greater than the normal component and both play a key role in the deformation-fracture of the main roof, unlike in the case of flat or gently dipping seams.

Some researchers have studied the stress-deformation-fracture characteristics of the main roof above a SCS.

Kulakov [3] determined the pattern of strata behavior induced by the mining of a SCS based on actual measurement, but the analysis focused only on various phenomena associated with strata behavior that had occurred at a working face. Bodi [4] discussed an unmanned mining technique for SCSs and the difficulties in controlling surrounding rocks, but his study was not thorough. Yin and Wang [5] derived the relationship between the length of a working face in a SCS and the location of the maximum roof deflection under the assumption that the load on the roof was uniformly distributed, but they did not analyze the stress-fracture characteristics of the roof. Yang [6] constructed a formula for estimating the deflection of the roof above a SCS using the small-deflection theory for elastic thin plates and the variational principle of minimum total potential energy revealing the movement-fracture mechanism of a roof above a SCS. Zhang et al. [7] obtained an analytical expression for roof deflection using the energy method in Kirchhoff's theory of elastic thin plates and discussed the deflection characteristics of the main roof, with the influence of an internal force acting on the middle plane taken into account. This research also analyzed how the dip angle of a coal seam and the thickness of the main roof depend on the amount of roof deflection. By treating the overburden as a rock plate, Yin et al. [8] investigated the deformation characteristics of overburden and created an overburden deformation model based on the theory of elasticity. A deflection equation for overburden disturbed by mining and a theoretical formula for predicting the location of the maximum deflection were derived. The results of calculations using the formulas showed that roof deflection was greater in the lower part of the goaf than in its upper part, and the maximum deflection occurred at a location in the lower middle part of the face. Li and Liu [9] modeled the roof above a SCS as a clamped-clamped beam parallel to the dip direction of the roof using a theoretical method and analyzed the forces acting on different locations of the roof. However, this analysis focused on the roof's deformation before it fractured and the mechanical model adopted was a simple two-dimensional model. In a mechanical analysis of the surrounding rocks disrupted by mining a SCS, Wu suggested that the fractured roof did not form any structure in the direction of advance of the working face. Along the length of the working face, the fractured roof stacked up into along-dip and antidip piles, but these piles were asymmetrically distributed at both ends of the face rather than forming a continuous structure to protect the stope below.

Previous research on the stress-deformation-fracture characteristics of the roof above a SCS largely used a beam or plate model to represent the roof and assumed that the load on the roof had a uniform or trapezoidal distribution, which cannot reflect the actual mechanical behavior of the roof above a SCS. In situ monitoring shows that as the mining in a SCS progresses, the immediate roof can cave easily and the caved rock then refills the lower part of the goaf [10, 11], leaving the upper section of the roof hanging above the goaf. As a result, the load on the overburden at the working face is asymmetrical in the dip direction (Figure 1), and

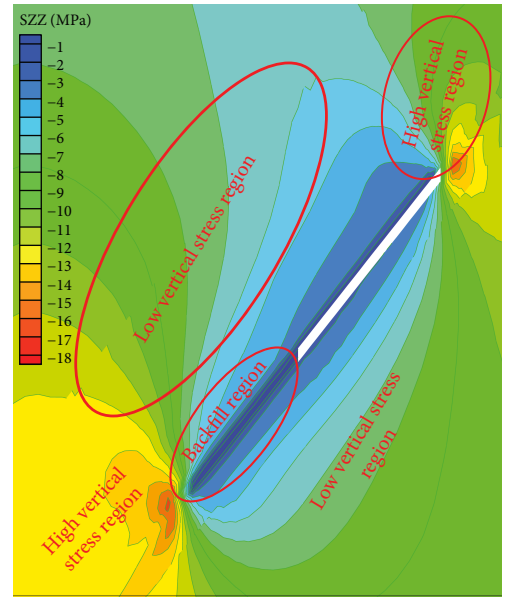

Figure 1: Stress distribution in a stope.

thus the bed separation and caving of the overburden are asymmetrical, adding to the difficulty of surrounding rock control [12, 13]. The support provided by the backfill in the goaf inevitably has an effect on the stress-deformation of the main roof of the working face in a SCS. However, this effect has not been examined in the aforementioned studies. For this reason, the current study first analyzed the characteristics of the caving of the immediate roof and backfill in the goaf during mining in a SCS and then investigated the stress-deformation-fracture characteristics of the main roof. The findings of the study can provide a helpful guide on how to control the surrounding rocks at working faces in SCSs based on an understanding of the characteristics of strata behavior.

2. Characteristics of Backfill in the Goaf

The supports are located at the coal wall of the working face and play a fixing role on the edge of the roof. This research is about the stress-deformation-fracture characteristics of the main roof in the goaf. However, according to the parameters (width 1.5 m, length 5.5 m and support resistance 2600 kN) of the supports in the Xintie Coal Mine, we can calculate the resistance pressure as 0.31 MPa, and this can be ignored compared with the weight of the roof overburden. So, this study did not consider the role of support resistance to the goaf roof.

During mining in a SCS, the immediate roof will collapse and refill the lower part of the goaf due to the large dip angle of the seam. Therefore, the roof caving height decreased roughly from the upper end to the lower end of the face. When the suspended section of the main roof above the goaf has a width smaller than the main roof's ultimate caving interval, the main roof, backfill, and the rock block along the upper section of the face can form an arch-shaped

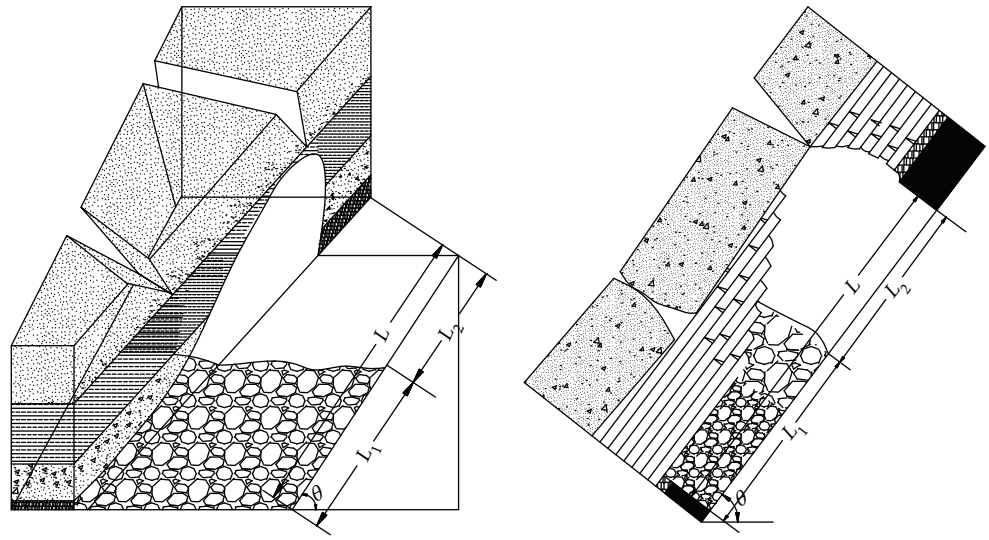

(a) Three-dimensional schematic (b) Profile along the dip direction

Figure 2: Schematic of the backfill in the goaf.

structure in mechanical equilibrium. The backfill along the lower section of the face then exerts an influence on the force-deformation properties of the roof of the face.

Based on the lithology and mechanical properties of the overburden, the immediate roof beneath the main roof can be divided into strata very prone to caving and hysteretic caving strata. Strata very prone to caving collapse readily as face supports advance. The suspended section of such strata behind the working face is usually shorter than the width of a single support (the width of a single support is 1.5 m) [14]. In contrast, hysteretic caving strata do not fall easily and their suspended sections are usually as long as 2-5 times the width of a single support [2]. As the roof supports advance in the order starting from the lowermost to the uppermost [15–17], the strata very prone to caving tend to fall immediately behind the supports, while the upper hysteretic caving strata collapse as the working face moves forward. The caved rock then refills the lower part of the goaf. The scope of the backfill in the goaf was determined based on the characteristics of caving and movement of the immediate roof. Figure 2 shows the schematic of the backfill in the goaf. In this figure, M is the mining height, L is the length of the working face, and L_1 is the width of the backfill in the lower part of the goaf.

To facilitate subsequent quantitative analysis, the cavity created by roof caving along the middle-upper part of the working face was simplified to a space with trapezoidal cross section in the dip direction, as shown in Figure 3. In Figure 3, L_3 represents the width of the backfill derived from the hysteretic caving strata, θ is the lower caving angle in the dip direction, and γ is the upper caving angle in the dip direction.

The problem of determining the width of the backfill in the goaf can be converted to solving for the length of the segment DI or EF shown in Figure 3(b). The length of AH is the thickness of the hysteretic caving strata denoted as H_2. The length of very prone to caving strata is denoted as H_1. The length of AB is then given by

$$\mathrm{AB} = L_2 + L_3 - \frac{H_2}{\tan\beta} - \frac{H_2}{\tan\gamma}. \tag{1}$$

Based on their geometrical relationship and equation (1), the lengths of CD, DE, and GF can be expressed as follows:

$$\begin{cases} \mathrm{CD} = L_2 + L_3, \\ \mathrm{DE} = H_1 + M, \\ \mathrm{GF} = L_3 \tan\beta + H_1 + M. \end{cases} \tag{2}$$

L_1, L_2, and L_3 can be related by the following equations:

$$\begin{cases} L_1 = \dfrac{LH_1k}{H_1 + M} + L_3, \\ L_2 = L - \dfrac{LH_1k}{H_1 + M} - L_3. \end{cases} \tag{3}$$

After bulking, the caved rock from the region defined by ABCD in the cross section then occupies the space defined by DEFG in the cross section, according to the geometrical relationship shown in Figure 3(b). Simultaneously solving equations (1), (2), and (3) yields the width of the backfill along the lower section of the working face:

$$L_1 = \frac{1}{\tan\beta + 2H_1 + 2M} \cdot \left[2LH_2k - \frac{2LH_1H_2k}{(H_1 + M)} - H_2^2k\left(\frac{1}{\tan\beta} - \frac{1}{\tan\gamma}\right)\right], \tag{4}$$

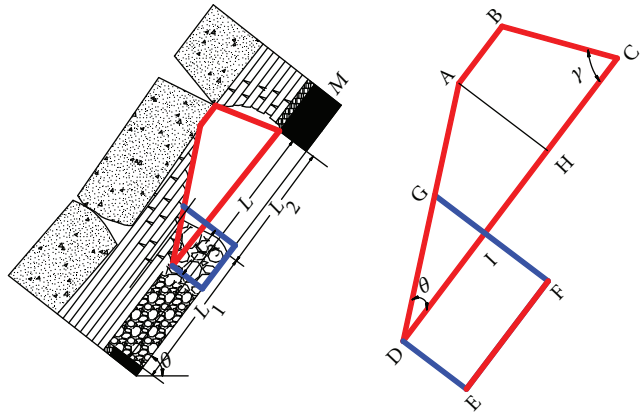

(a) Sketch drawn (b) Geometrical relationship

Figure 3: Sketch of roof caving and the backfill in the goaf.

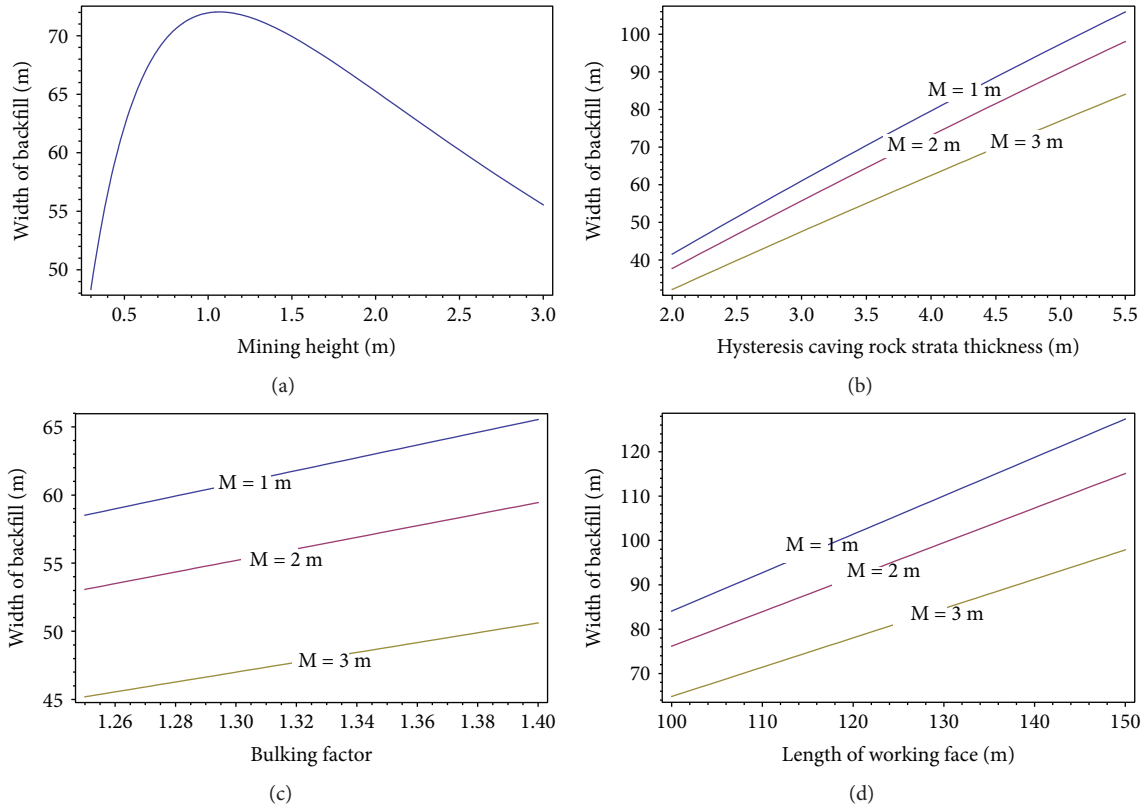

Figure 4: Variation in the width of the backfill with different operational parameters.

where k is the bulking factor of the caved rock, normally ranging from 1.25 to 1.5. In the Xintie Coal Mine, the working face is 115 m long and has a mining height of 1.6 m. The lower and upper caving angles are 28° and 59°, respectively. The curves in Figure 4 were obtained from equations (1), (2), (3), and (4) to illustrate the effects of different operational parameters on the width of the backfill.

Figure 4 demonstrates that the width of the backfill increases linearly with the increasing thickness of hysteretic caving strata, bulking factor of caved rock, and length of working face. As the mining height increases, the width of the backfill in the lower part of the goaf increases rapidly and peaks when the mining height reaches 1 m, followed by a slow decrease. Since the thickness of a SCS at a fully mechanized face is normally greater than 1 m, it follows that the width of the backfill tends to increase with the increasing thickness of hysteretic caving strata, bulking factor of caved rock, and length of working face and decreases with increasing mining height in actual mining.

3. Force-Deformation Model of Roof above SCS

According to the theory of elastic thin plates, a plate can be treated as a thin plate if the ratio of its thickness to its

minimum width is greater than 1/100 to 1/80 and less than 1/8 to 1/5 [18, 19]. This theory is applicable if the ratio of the roof thickness to the length of the working face or roof caving interval satisfies this condition [20].

3.1. Mechanical Analysis of Roof above SCS. A mechanical analysis shows that the force exerted by overlying strata and the support provided by the backfill in the lower part of the goaf are the main forces that cause the main roof to deform. The force exerted by overlying strata consists of two components: a shear component parallel to the dip direction and a normal component. Due to the large dip angle, the shear component is greater than the normal component and thus nonnegligible. It is reasonable to infer that the deformation of the roof of the working face in a SCS is caused by the action of both the shear and normal loads.

The rectangular coordinate system shown in Figure 5 was established to enable the integration involved in the problem-solving process to start from the origin. In this figure, a denotes the roof width in the x direction, i.e., the breaking length of the roof; b denotes the roof width in the y direction, i.e., the length of working face in the dip direction; q represents the force exerted by overlying strata, which has a trapezoidal distribution; H_3 is the burial depth of the seam at the upper end of the working face; H_4 is the seam's burial depth of the seam at the lower end of the working face; q_1 is the force on the roof's upper end, defined by $q_1 = \gamma H_3$; q_2 is the force on the roof's upper end, defined by $q_2 = \gamma H_4$; and γ is the average body force on the strata. Then, the force exerted by overlying strata can be expressed as $q = q_2 - (q_2 - q_1)y/b$; its normal component is $q_{11} = q\cos\theta$ and shear component is $q_{12} = q\sin\theta$, with θ indicating the dip angle of the seam.

In the lower part of the goaf behind the working face, the caved rock backfill experiences compressive deformation partly as a result of the movement of overburden. Coordinated interaction exists between the overlying strata and backfill. As the amount of downward deflection of overburden increases, the backfill tends to be compacted to a greater degree, have a higher bearing capacity, and thus be able to provide a greater force to support the roof.

Mechanical tests on backfill samples have shown that the behavior of the backfill in triaxial compression can be divided into four stages: elastic deformation, yielding, plastic deformation, and plastic failure, and the stress in the backfill was asymmetric along the width of the backfill [21]. If a plate's deflection is relatively small according to the criterion set out in the small-deflection theory for thin plates, Winkler's assumption that the reaction force provided by an elastic foundation per unit area is directly proportional to the plate's deflection at the point of interest applies [22]. In this case, the load on the backfill in the goaf derived from the roof can be expressed in the following form:

$$F = k_1 w, \tag{5}$$

where F is the force provided by the backfill (N); k_1 is the equivalent elastic constant (MPa/m); and w is the main roof's deflection (m).

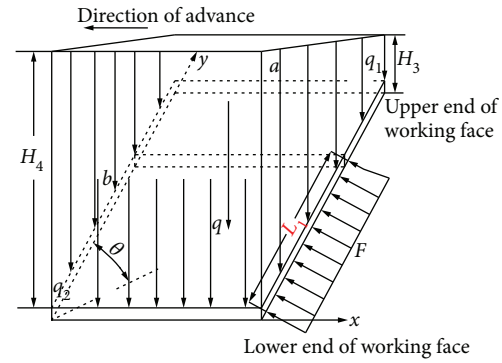

Figure 5: A working face model for the mechanical analysis of the main roof.

Let w_1 be the roof deflection caused by q_{11}, w_2 be the roof deflection caused by q_{12}, and w_3 denote the deflection attributed to F. According to the superposition principle, the total roof deflection is the sum of the three: $w = w_1 + w_2 + w_3$.

3.2. Roof Deflection Equation. According to the theory of elastic thin plates, a thin plate's deformation is negligible when it is subjected to only a load parallel to the plate's plane, but the action of normal and shear loads combined can cause considerable deformation [18]. In the latter case, the thin plate first undergoes deformations caused by normal loads, w_1 and w_3, followed by deformation due to shear load, w_2. The deformation of a thin plate under both shear and normal loads can be described by the following differential equation of static equilibrium:

$$D\nabla^4\omega = q_r + N_x\frac{\partial^2\omega}{\partial x^2} + 2N_{xy}\frac{\partial^2\omega}{\partial x\partial y} + N_y\frac{\partial^2\omega}{\partial y^2}, \tag{6}$$

where D is the flexural rigidity of the thin plate, defined by $D = Eh^3/12(1-\nu^2)$; E is the elastic modulus of the thin plate; h is plate thickness; ν is Poisson's ratio of the plate; w is the deflection function for the plate; q_r is the normal load on the plate; and N_x, N_y, and N_{xy} are internal forces acting within the thin plate across three internal surfaces, respectively. The three interval forces can be expressed as follows: $N_x = h\sigma_x$, $N_y = h\sigma_y$, and $N_{xy} = h\tau_{xy}$. Then, the relationship between w_1, w_2, and w_3 can be written as follows [14]:

$$D\nabla^4\omega_2 = q_{r1} + q_{r3} + N_x\frac{\partial^2\omega_2}{\partial x^2} + 2N_{xy}\frac{\partial^2\omega_2}{\partial x\partial y} + N_y\frac{\partial^2\omega_2}{\partial y^2}, \tag{7}$$

where $q_{r1} = N_x\partial^2\omega_1/\partial x^2 + 2N_{xy}\partial^2\omega_1/\partial x\partial y + N_y\partial^2\omega_1/\partial y^2$ and $q_{r3} = N_x\partial^2\omega_3/\partial x^2 + 2N_{xy}\partial^2\omega_3/\partial x\partial y + N_y\partial^2\omega_3/\partial y^2$. The first step to solve the problem is to calculate w_1 and w_3. According to the solution of the classical theory of elastic thin plates

(Navier solution), we can assume that the deflection w_1 has the following functional form:

$$\omega = \sum_{m=1}^{\infty}\sum_{n=1}^{\infty} A_{mn} \sin^2\frac{m\pi x}{a} \sin^2\frac{n\pi y}{b}, \tag{8}$$

where A_{mn} is an undetermined coefficient and m and n are arbitrary positive integers, which can be determined based on the convergence of the series and the accuracy requirements of a specific project. At the beginning of mining at a working face in a SCS, the roof can be viewed as a rectangular plate with four clamped edges and the corresponding boundary conditions are $(\omega)_{x=0,a} = (\partial\omega/\partial x)_{x=0,a} = 0$ and $(\omega)_{y=0,b} = (\partial\omega/\partial y)_{y=0,b} = 0$. It is obvious that the deflection equation (8) satisfies these boundary conditions. Assuming that q_{11} is the only load acting on the roof, then $N_x = 0$, $N_y = 0$, and $N_{xy} = 0$. Substituting equation (8) into equation (6) yields

$$\begin{cases} \omega_1 = A_{mn} \sum\limits_{m=1,2,\ldots}^{\infty}\sum\limits_{n=1,2,\ldots}^{\infty} \sin^2\dfrac{m\pi x}{a} \sin^2\dfrac{n\pi y}{b}, \\ A_{mn} = \dfrac{(q_1+q_2)\cos\theta}{\pi^4 D\left(3m^4/a^4 + 2m^2n^2/a^2b^2 + 3n^4/b^4\right)}. \end{cases} \tag{9}$$

The deformation of the backfill in equation (5) is equal to the roof deflection caused by the normal load q_{11}. Similarly, the roof deflection attributed to F can be written as

$$\begin{cases} \omega_3 = C_{mn} \sum\limits_{m=1,2,\ldots}^{\infty}\sum\limits_{n=1,2,\ldots}^{\infty} \sin^2\dfrac{m\pi x}{a} \sin^2\dfrac{n\pi y}{b}, \\ C_{mn} = -\dfrac{3(q_1+q_2)k\cos\theta}{64\pi^9 nD^2\left(3m^4/a^4 + 2m^2n^2/a^2b^2 + 3n^4/b^4\right)^2}\left(\dfrac{12L_1n\pi}{b} - 8\sin\dfrac{2L_1n\pi}{b} + \sin\dfrac{4L_1n\pi}{b}\right). \end{cases} \tag{10}$$

Previous mechanical analyses indicate that roof deformation caused by a normal load is much greater than that caused by a shear load [18]. As the first two terms on the right-hand side of equation (7) have values significantly greater than those of the latter three terms, the latter three terms can be omitted and then equation (7) can be reduced to a simpler form:

$$D\nabla^4\omega_2 = q_{r1} + q_{r3} = q_{r2}. \tag{11}$$

The mechanical model shown in Figure 5 reveals that the displacement of the midsurface of the thin plate is not constrained by the boundary conditions on the x-axis and the plate's top surface. Thus, the forces on the midsurface can be expressed as follows:

$$\begin{cases} N_x = h\sigma_x = 0, \\ N_y = h\sigma_y = -q_{12}y = \left(q_2 - \dfrac{q_2 - q_1}{b}y\right)\sin\theta, \\ N_{xy} = h\tau_{xy} = 0. \end{cases} \tag{12}$$

Then, we have

$$\begin{aligned} q_{r2} &= N_y\frac{\partial^2\omega_1}{\partial^2 y} + N_y\frac{\partial^2\omega_3}{\partial^2 y} \\ &= N_y(A_{mn} + C_{mn}) \\ &\quad \cdot \sum_{m=1,2,\ldots}^{\infty}\sum_{n=1,2,\ldots}^{\infty} \frac{2\pi^2n^2}{b^2}\cos\frac{2n\pi y}{b}\sin^2\frac{m\pi x}{a}\sin^2\frac{n\pi y}{b}. \end{aligned} \tag{13}$$

The roof deflection caused by the shear load can be obtained using the solution for the deflections caused by the normal loads:

$$\begin{cases} \omega_2 = B_{mn} \sum\limits_{m=1,2,\ldots}^{\infty}\sum\limits_{n=1,2,\ldots}^{\infty} \sin^2\dfrac{m\pi x}{a} \sin^2\dfrac{n\pi y}{b}, \\ B_{mn} = \dfrac{3a^8b^8\cos(q_1+q_2)\sin 2\theta\left(\left(-15+8n^2\pi^2\right) + \left(15+4n^2\pi^2\right)\right)}{32768\pi^{14}n^2D^3\left(3b^2m^4 + 2a^2b^2m^2n^2 + 3a^2n^4\right)^3} \times \left(4n\pi\left(-9a^4b^3kL_1 + 8D\left(3b^2m^4 + 2a^2b^2m^2n^2 + 3a^2n^4\right)\pi^4\right) - 3a^4b^4k\left(-8\sin\dfrac{2L_1n\pi}{b} + \sin\dfrac{4L_1n\pi}{b}\right)\right). \end{cases} \tag{14}$$

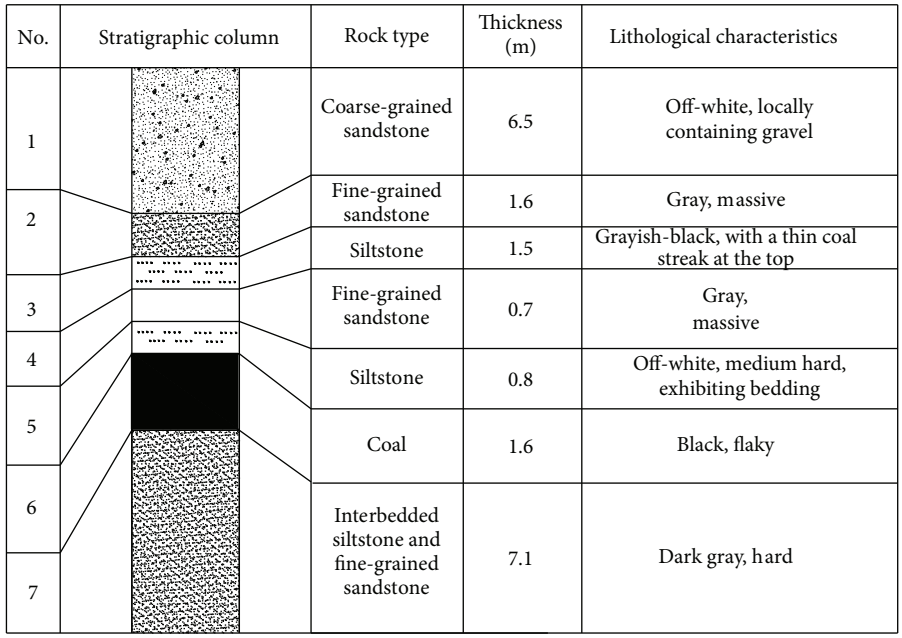

No.	Stratigraphic column	Rock type	Thickness (m)	Lithological characteristics
1		Coarse-grained sandstone	6.5	Off-white, locally containing gravel
2		Fine-grained sandstone	1.6	Gray, massive
		Siltstone	1.5	Grayish-black, with a thin coal streak at the top
3		Fine-grained sandstone	0.7	Gray, massive
4		Siltstone	0.8	Off-white, medium hard, exhibiting bedding
5		Coal	1.6	Black, flaky
6		Interbedded siltstone and fine-grained sandstone	7.1	Dark gray, hard
7				

Figure 6: Composite stratigraphic column.

High solution accuracy is not required for problems in mining engineering. When $m = 1$ and $n = 1$, these equations can provide roof deflection estimates with the desired accuracy [23]. Therefore, the total deflection of the roof above a SCS can be described by the following equation:

$$\omega = \omega_1 + \omega_2 + \omega_3 = (A_{mn} + B_{mn} + C_{mn}) \sum_{m=1,2,\ldots}^{\infty} \sum_{n=1,2,\ldots}^{\infty} \sin^2 \frac{m\pi x}{a} \sin^2 \frac{n\pi y}{b}. \quad (15)$$

The mechanical characteristics of the roof above a SCS indicate that the distribution of forces on the roof is symmetrical about the bimedian of the rectangular roof perpendicular to the strike direction and is asymmetrical in the dip direction. Then, substituting $x = a/2$ into equation (15) and computing the derivative of y will give the y-coordinate of the location showing the maximum roof deflection.

4. Case Study

4.1. Project Overview. The Xintie Coal Mine analyzed in this section is operated by the Qitaihe branch of Heilongjiang LongMay Mining Holding Group Co. Ltd. More than 50% of its coal seams are steep seams, which have 95.57 million tons of coal reserves. The main seam being worked is the steeply dipping #49 seam, where coal is extracted from the Zuoqipian working face in the 5th district of the 1st mining level. It is 1.6 m thick on average (Figure 6), has a stable and simple structure, and dips at 53° to 57°, with an average of 55°. Its elevation ranges from -153 m to -241 m and the surface above it has an elevation of +219 m. The coal hardness is measured at 0.8. The Zuoqipian working face is parallel to the dip direction of the seam and advances in the strike direction. The panel being mined measures 115 m in the dip direction and 310 m in the strike direction. The immediate roof, with an average thickness of 4.6 m, consists of siltstone and fine-grained sandstone. The main roof, 6.5 m thick on average, is composed of interbedded coarse-grained sandstone and fine-grained sandstone. The main floor, 7.1 m thick on average, is made up of interbedded siltstone and fine-grained sandstone. The coal is cut from this working face from the upper end to the lower end by a MG2 × 125/580-WD shearer and transported by a SGZ-730/320 scraper chain conveyor. ZQY2600/12/26 hydraulic supports are used to control the fall of the roof.

4.2. Stress Distribution in Roof. The stratigraphic column shown in Figure 6 suggests that the hysteretic caving strata in the immediate roof are 3.1 m thick, and the strata very prone to caving are 1.5 m thick. The length of the working face is 115 m, and the mining height is 1.6 m. The width of the backfill in the lower part of the goaf behind the face estimated by equation (4) is 63 m.

The first weighting interval of the main roof was measured at 57 m during actual mining. The coal seam dips at 55° on average and is 372 m deep at the upper end of the face and 460 m deep at the lower end of the face. The main roof has a thickness of 6.5 m, Poisson's ratio υ of 0.25, and equivalent elastic constant k of 30 MPa/m [24]. The average body force acting throughout the main roof, γ, is 25 kN/m^3. Based on the deformation-stress

relationship of thin plates, the distribution of normal and shear stresses in the main roof can be expressed as follows:

$$\begin{cases} \sigma_x = -\dfrac{E}{1-\upsilon^2}\left(\dfrac{\partial^2\omega}{\partial x^2} + \upsilon\dfrac{\partial^2\omega}{\partial y^2}\right), \\ \sigma_y = -\dfrac{E}{1-\upsilon^2}\left(\dfrac{\partial^2\omega}{\partial y^2} + \upsilon\dfrac{\partial^2\omega}{\partial x^2}\right), \\ \tau_{xy} = -\dfrac{E}{1+\upsilon^2}\dfrac{\partial^2\omega}{\partial x\partial y}. \end{cases} \tag{16}$$

Substituting the abovementioned parameter values into equation (15) and then solving equations (15) and (16) give the distribution of stress in the roof above the SCS, which is presented in Figure 7. The stress levels shown in this figure are expressed in MPa.

As Figure 7 shows, the distribution of coplanar stress in the dip direction (y direction) is apparently asymmetrical, while the horizontal stress parallel to the strike direction (x direction) is symmetrical about the bimedian of the rectangular roof perpendicular to the strike direction. The shear stresses in the lower roof section are relatively low due to the support provided by the backfill in the lower part of the goaf. The upper roof section which hangs above the goaf exhibits relatively high shear stresses due to the absence of external support. Moreover, the shear stress in the strike direction is greater than the shear stress in the dip direction. The horizontal stress peaks in three locations: the midpoint of the suspended roof section above the goaf, the upper section of the wall in front of the face (frontal wall), and the upper section of the wall behind the goaf (rear wall). Overall, shear stress is locally concentrated in the roof and has symmetrical distribution along the length of the working face and asymmetrical distribution along the advance direction of the face. Peak shear stresses occur at the centers of the stress concentration regions.

4.3. Distribution Characteristics of Roof Deformation and Fracture. According to various failure criteria, the fracture of a material should first take place at the location of maximum principal stress. The relationships between principal stress, normal stress, and shear stress are governed by the following equations [18]:

$$\begin{aligned} \left.\begin{matrix} \sigma_{\max} \\ \sigma_{\min} \end{matrix}\right\} &= \frac{\sigma_x + \sigma_y}{2} \pm \sqrt{\frac{\left(\sigma_x - \sigma_y\right)^2}{2} + \tau_{xy}^2}, \\ \tau_{\max} &= \frac{\sigma_{\max} - \sigma_{\min}}{2}. \end{aligned} \tag{17}$$

These equations can be used to predict the distribution of maximum principal stress and maximum shear stress.

Figures 8 and 9 show the distribution patterns of the maximum principal stress and maximum shear stress, respectively, in the roof under study. In these figures, a negative value indicates that the stress has a direction opposite to that of the principal stress (positive values represent compressive stress while negative values represent tensile stress). As can be seen in the figures, the maximum principal stress is concentrated in the upper sections of the frontal and rear walls of the working face. It is a tensile stress and peaks at about 7 MPa. The maximum compressive stress is concentrated in the middle of the upper suspended roof section and peaks at around 2 MPa. The lower roof section experiences relatively low stresses due to the support provided by the caved rock. Shear stress is greater in the upper roof section than in the lower section. The maximum shear stress is distributed in the upper sections of the frontal wall and rear wall as well as in the middle of the suspended roof section, peaking at about 1.8 MPa.

Normally, the compressive strength of a rock is significantly greater than its tensile strength and is also greater than its shear strength. This, combined with the characteristics of stress distribution in the roof, suggests that the upper sections of the frontal wall and rear wall and the middle of the upper roof section may first fracture due to tension or shearing. The fractures in the three locations will interconnect to form an E-shaped pattern and propagate downslope through the strata, as illustrated in Figure 10. Figure 11 shows the three-dimensional distribution of deflection of the roof in the Xintie Coal Mine predicted by the deflection equation proposed in this study.

Figure 11 reveals that the distribution of the roof deformation at the Zuoqipian working face is symmetrical about the bimedian of the rectangular roof perpendicular to the strike direction. In the dip direction, the roof deformation is largely concentrated at the upper section of the face. The maximum deformation is around 0.8 m and occurs at a location 39 m from the upper end of the working face.

Data on support pressure measured during mining can provide qualitative information about roof deformation. To validate the deformation distribution obtained by theoretical calculation, 5 observation stations (Figure 12), numbered 1 through 5, were laid out downslope along the dip direction and 3 groups of pressure gauges were installed at each station to measure rock pressure for one month. The rock pressure data for nearly one month (over which the working face advanced 124 m) was used to analyze the distribution of pressure on hydraulic supports along this face. The pattern of support pressure distribution at this face is demonstrated in Figure 13, which only provides the average support pressure at each station.

The measurements of support pressure suggest that the supports along the middle section of the working face experienced the highest pressure, followed by those along the upper section. The supports along the lower section of the working face were subject to the lowest pressure, which was roughly equal to the pressure at the pump station. A greater amount of roof deformation was associated with a higher pressure on roof support. This consistency indirectly confirms the accuracy of the pattern of roof deformation determined by theoretical analysis.

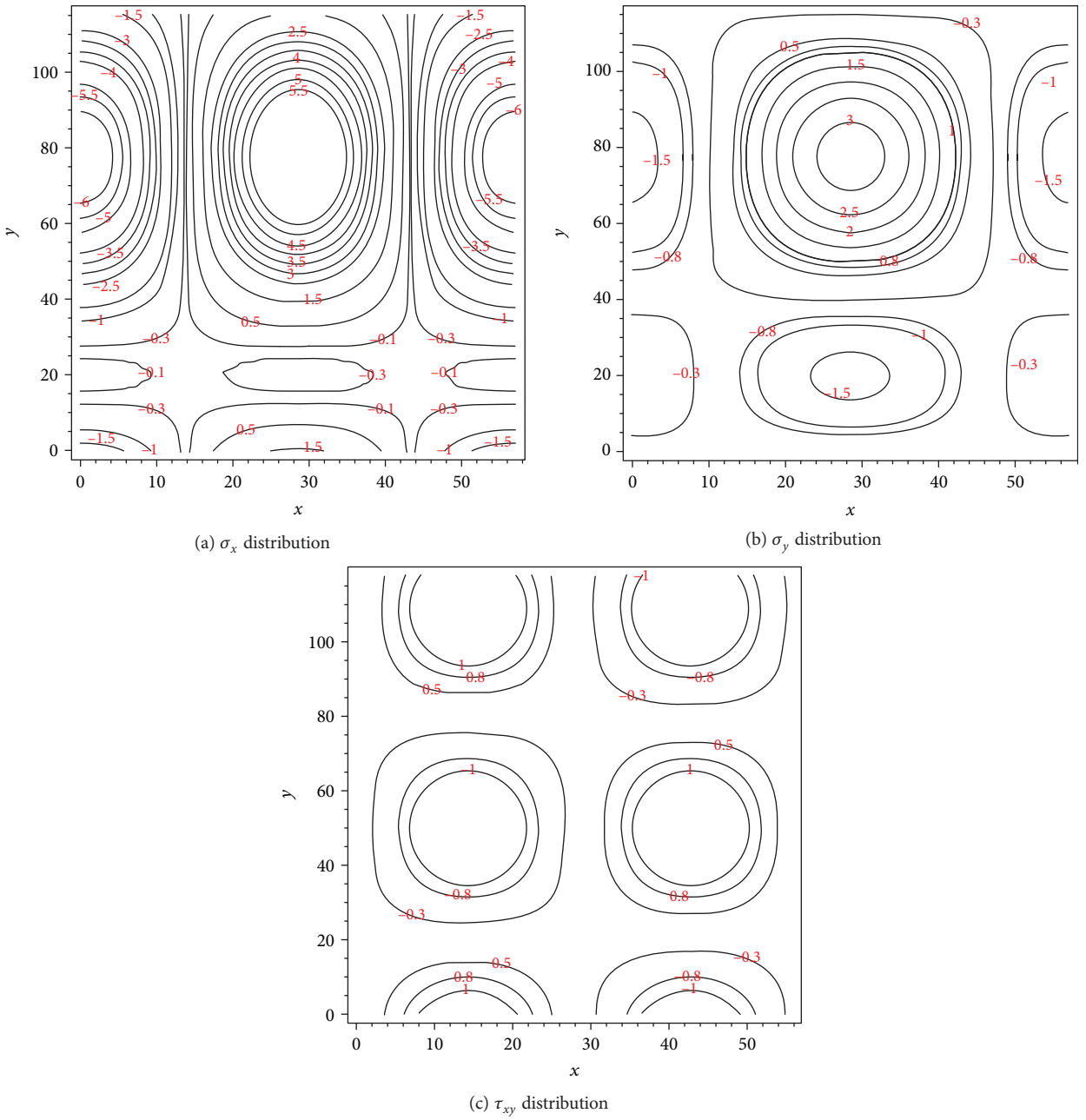

(a) σ_x distribution

(b) σ_y distribution

(c) τ_{xy} distribution

Figure 7: Stress distribution in the roof in different directions.

5. Conclusions

(1) The immediate roof of a working face in a SCS can be divided into strata very prone to caving and hysteretic caving strata, based on the lithology and ability of immediate roof strata to cave. A formula for calculating the width of the backfill in the lower part of the goaf behind the working face was derived. The main factors affecting the backfill width were analyzed.

(2) A mechanical model of a working face above a SCS was constructed based on the theory of elastic thin plates. A roof deflection equation was obtained for estimating the roof deformation under the load from overlying strata combined with the support provided by the backfill in the goaf.

(3) A case study of the Zuoqipian working face in the #49 seam of the Xintie Coal Mine shows that the lower section of the roof experiences relatively low levels of stress while the upper section of the roof exhibits high levels of stress. The upper sections of the frontal and rear walls of the working face and the middle of the upper section of the roof show relatively high

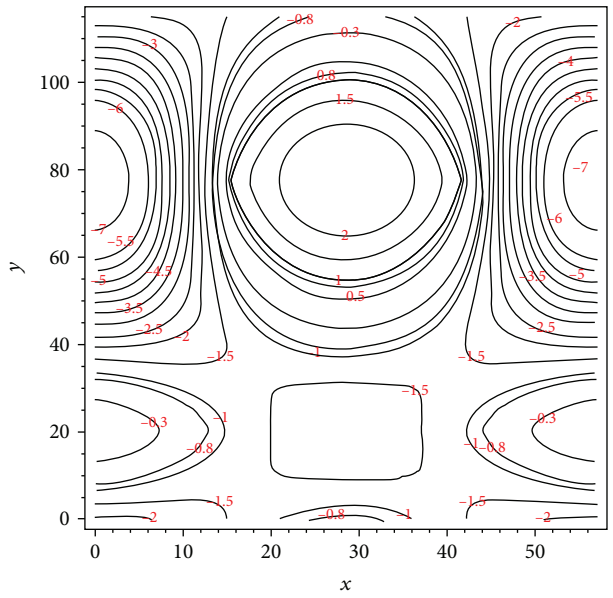

Figure 8: Distribution of maximum principal stress.

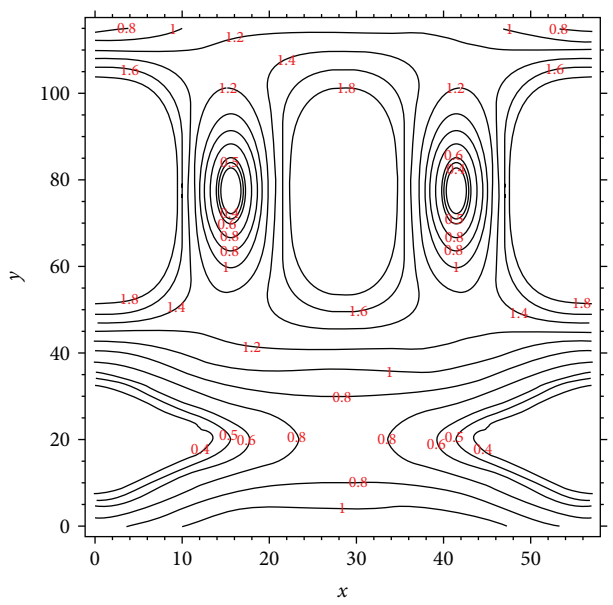

Figure 9: Distribution of maximum shear stress.

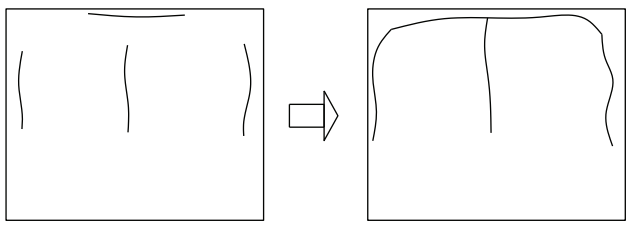

Figure 10: Pattern of roof fractures.

levels of tensile stress and shear stress. The fractures in the roof may form an *E*-shaped pattern and propagate downslope through the strata.

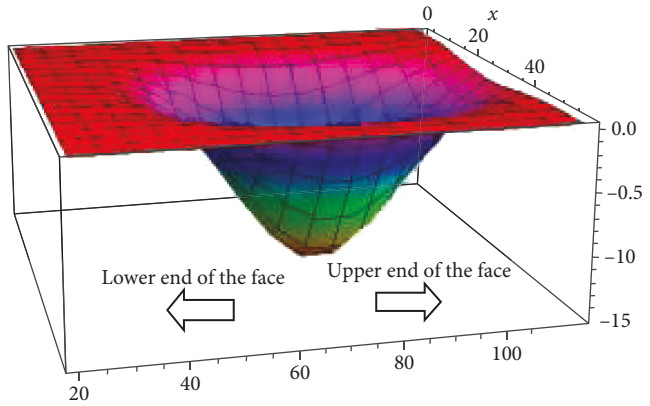

Figure 11: Three-dimensional distribution of roof deflection.

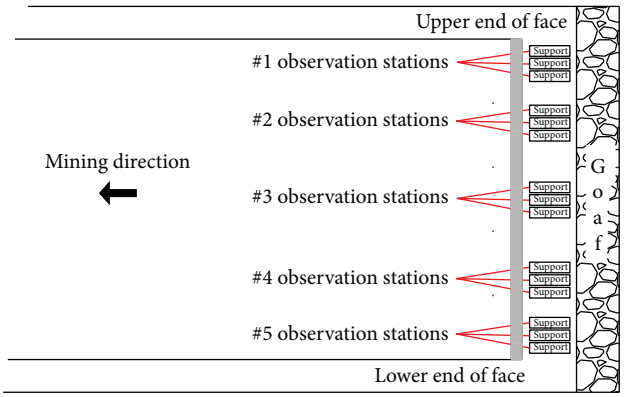

Figure 12: Distribution of observation stations along the dip direction.

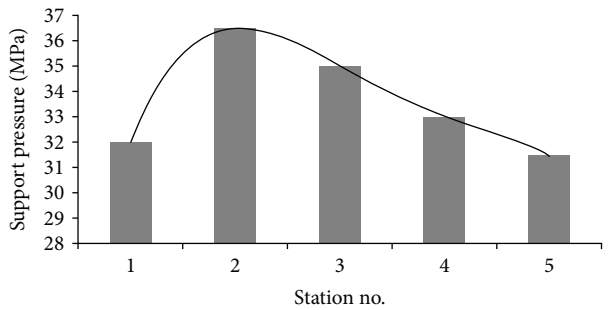

Figure 13: Distribution of support pressure along the dip direction.

(4) According to the theoretical analysis combined with the actual operational parameters of the Zuoqipian working face, the maximum roof deflection is around 0.8 m and occurs at a location 39 m from the upper end of the working face. The roof deformation obtained by theoretical analysis and the measured support pressure follow a similar distribution pattern, thus confirming the accuracy of the theoretical results.

Data Availability

The data used to support the findings of this study are available from the corresponding author upon request.

Conflicts of Interest

The authors declare that they have no conflicts of interest.

Acknowledgments

The authors gratefully acknowledge the financial support from the National Key R&D Program of China (2018YFC0604701) and the Independent Research Project of the State Key Laboratory of Coal Resources and Safe Mining, CUMT (SKLCRSM18X003).

References

[1] W. Wang, H. Wang, D. Li, H. Li, and Z. Liu, "Strength and failure characteristics of natural and water-saturated coal specimens under static and dynamic loads," *Shock and Vibration*, vol. 2018, Article ID 3526121, 15 pages, 2018.

[2] M. G. Qian and P. W. Shi, *Underground Pressure and Strata Control*, China University of Mining and Technology Press, Xuzhou, China, 2003.

[3] V. N. Kulakov, "Stress state in the face region of a steep coal bed," *Journal of Mining Science*, vol. 31, no. 3, pp. 161–168, 1995.

[4] J. Bodi, "Safety and technological aspects of manless exploitation technology for steep coal seams," in *27th International Conference of Safety in Mines Research Institutes*, pp. 955–965, New Delhi, India, 1997.

[5] L. Z. Yin and W. Wang, "Primary exploration of deflection displacement in the condition of large dip angle roof ahead of first fracture," *Ground Pressure and Strata Control*, vol. 3, pp. 21–23, 1996.

[6] F. Yang, *Study on Overburden Strata's Movement Pattern and Mechanism of Mining Steeply Inclined Seams, [M.S. thesis]*, Liaoning Technical University, Liaoning, China, 2006.

[7] J. F. Zhang, P. W. Shi, and H. M. Zang, "Stability analysis of basic roof after first destruction in the steep seam," *Journal of China Coal Society*, vol. 34, no. 9, pp. 1160–1164, 2009.

[8] G. Z. Yin, D. K. Wang, and W. Z. Zhang, "Mechanics model to deformation of covered rock strata and its application in deep mining of steep or inclined seam," *Journal of Chongqing University*, vol. 29, no. 2, pp. 79–82, 2006.

[9] X. M. Li and F. Liu, "Analysis of overlying strata structure and strata behavior characteristics of stope in steep coal seam," *Coal Engineering*, vol. 48, no. 5, pp. 80–83, 2016.

[10] Y. P. Wu, P. S. Xie, and S. G. Ren, "Analysis of asymmetric structure around coal face of steeply dipping seam mining," *Journal of China Coal Society*, vol. 35, no. 2, pp. 182–184, 2010.

[11] H. S. Tu, *Overlying Strata Movement Law and Control Mechanism of Fully Mechanised Longwall Mining Face in Thin and Medium Thickness Steeply Inclined Coal Seam, [M.S. thesis]*, China University of Mining and Technology, Xuzhou, China, 2014.

[12] C. Ross, D. Conover, and J. Baine, "Highwall mining of thick, steeply dipping coal—a case study in geotechnical design and recovery optimization," *International Journal of Mining Science and Technology*, 2018.

[13] J. Toraño, R. Rodríguez, and P. Ramírez-Oyanguren, "Probabilistic analysis of subsidence-induced strains at the surface above steep seam mining," *International Journal of Rock Mechanics and Mining Sciences*, vol. 37, no. 7, pp. 1161–1167, 2000.

[14] A. Asadi, K. Shahriar, K. Goshtasbi, and K. Najm, "Development of a new mathematical model for prediction of surface subsidence due to inclined coal-seam mining," *Journal of the South African Institute of Mining and Metallurgy*, vol. 105, no. 1, pp. 15–20, 2005.

[15] A. D. Alexeev, V. N. Revva, N. A. Alyshev, and D. M. Zhitlyonok, "True triaxial loading apparatus and its application to coal outburst prediction," *International Journal of Coal Geology*, vol. 58, no. 4, pp. 245–250, 2004.

[16] D. Yun, Z. Liu, W. Cheng, Z. Fan, D. Wang, and Y. Zhang, "Monitoring strata behavior due to multi-slicing top coal caving longwall mining in steeply dipping extra thick coal seam," *International Journal of Mining Science and Technology*, vol. 27, no. 1, pp. 179–184, 2017.

[17] J. Zhang and B. Shen, "Coal mining under aquifers in China: a case study," *International Journal of Rock Mechanics and Mining Sciences*, vol. 41, no. 4, pp. 629–639, 2004.

[18] B. L. Fu, *The Reciprocal Theorem is Bending Thin Plate*, Science Press, 2003.

[19] E. Ventsel and T. Krauthammer, *Thin Plates and Shells: Theory: Analysis, and Applications*, CRC Press, 2001.

[20] F. Yang, A. C. M. Chong, D. C. C. Lam, and P. Tong, "Couple stress based strain gradient theory for elasticity," *International Journal of Solids and Structures*, vol. 39, no. 10, pp. 2731–2743, 2002.

[21] Z. Guo and W. Huang, "Parameter optimization and stability analysis of inclined gangue strip-fillings," *Journal of China Coal Society*, vol. 36, no. 2, pp. 234–238, 2011.

[22] Q. Zong and W. Xu, "Analytical approach for prestressed anchor embedded in non-homogeneous stratum based on Winkler's assumption," *Rock and Soil Mechanics*, vol. 4, p. 10, 2009.

[23] A. E. H. Love, *A Treatise on the Mathematical Theory of Elasticity*, Cambridge University Press, 2013.

[24] G. L. He, D. C. Li, Z. W. Zhai, and G. Tang, "Analysis of instability of coal pillar and stiff roof system," *Journal of China Coal Society*, vol. 32, no. 9, pp. 897–901, 2007.